Tetraxial textiles: assessment of mesoscale mechanical modelling by experimental measurements

IOP Conf. Series: Materials Science and Engineering **406** (2018) 012048 doi:10.1088/1757-899X/406/1/012048

Tetraxial textiles: assessment of mesoscale mechanical modelling by experimental measurements

M Ghazimoradi[1], N Naouar[2], V Carvelli[1], P Boisse[2], R Frassine[3]

[1]Department A.B.C., Politecnico di Milano, Milan, Italy
[2]LaMCoS UMR 5259, INSA-Lyon, Université de Lyon, Villeurbanne, France
[3]Department of Chemistry, Materials and Chemical Engineering, Politecnico di Milano, Italy

Abstract. Tetraxial technical textiles were recently manufactured by a new loom developed to weave yarns in four directions. The textile has warp, weft, and two diagonal yarns oriented at symmetrical angles (typically ±45°) with respect to the warp direction. The peculiar yarns distribution could enhance the mechanical response of the textile in multiple directions aiming to almost isotropic in-plane behaviour. For the prediction of the mechanical performance of such tetraxial textiles, a reliable and accurate predictive model is of relevant importance. The present investigation aims to adopt the finite element numerical approach at the mesoscopic scale to predict the mechanical response for any in-plane loading of tetraxial textiles. An accurate modelling of the constitutive behaviour of the fibrous yarns was adopted considering a hyperelastic model. The modelling of the tetraxial unit cell allowed to have the mechanical behaviour for uniaxial and biaxial tensile and for shear loading conditions. The assessment of the accuracy of the numerical model was performed considering a huge experimental campaign dedicated to several hybrid tetraxial textiles. The comparison highlights the accuracy of the numerical model to predict the nonlinear behavior of the fabric for any loading condition and to provide the proper mechanical model for further optimization of tetraxial textiles supposed for different industrial applications.

1. Introduction

Woven fabrics with special architecture have received considerable attention in literatures [1], [2], due to their mechanical behaviour allowing for peculiar tear resistance as well as improved formability characteristics. Two-dimensional (2D) and three-dimensional (3D) fabric architectures can be considered in classification of technical textiles, which have more than two weaving directions. For instance, triaxial braiding produces a 2D architecture with three interlaced yarns; such fabrics have axial yarns in the longitudinal direction and the braided yarns tilted at an angle ranging from 30 to 60 with respect to the previous ones [3]. Advantages of triaxial braided fabrics are geometry flexibility and good tear resistance. Increasing the number of weaving direction to four, a 2D multiaxial textile is obtained, named tetraxial. The fabric architecture combines a traditional orthogonal interlacement with two additional threads (bias), which can be oriented at different angles with respect to the warp/weft direction (Figure 1). It has warp, weft, and two diagonal yarns oriented at symmetrical angles (typically 45°) with respect to the warp direction.

This study has two main parts; experimental and numerical. The first part, an extensive experimental campaign was conducted on tetraxial fabrics made of different yarns. Tensile and friction properties of the yarns were determined, as well as uniaxial and biaxial in-plane tensile tests of the fabric.

In the second part, a numerical model was adopted to predict the mechanical behaviour of tetraxial textiles varying several parameters, namely: material and spacing of the yarns. The meso-scale model takes into account the realistic geometry of woven structure, and the interaction between yarns. Furthermore a hyperelastic model has been adopted [5] considering four different deformation modes. The mesoscopic FE modelling of the tetraxial representative volume (RV) allowed simulating the mechanical behaviour for uniaxial, biaxial, and in-plane shear deformations. Finally, the comparison highlights the accuracy of the meso-scale FE model to predict the nonlinear behaviour of the fabric for any loading condition.

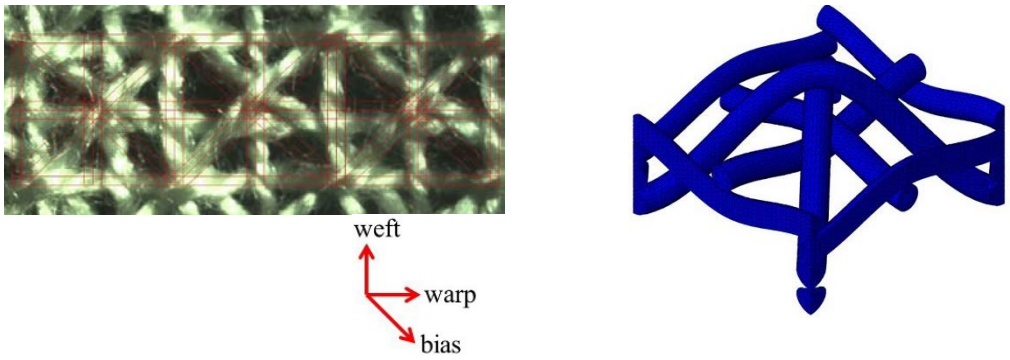

(a) (b)

Figure 1. (a) Tetraxial woven fabric, (b) sketch of the interlacement in the unit cell.

2. Textile features

The tetraxial machine, depicted in Figure 2, is a combination of a traditional woven machine (lower part, Figure 2a), and a specific automatic tension system (upper part, Figure 2b).

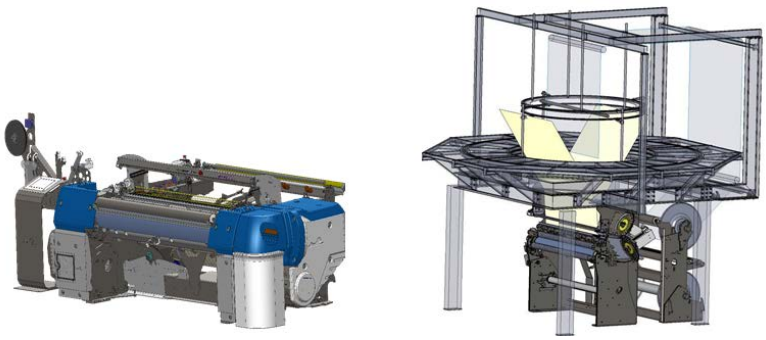

(a) (b)

Figure 2. Scheme of (a) lower and (b) upper part of the tetraxial loom.

The fabric can be considered as a combination of a traditional orthogonal fabric with two additional threads (bias), which can be oriented at different angles with respect to the warp directions (see Figure 1b).

Table 1. Some features of the tetraxial textile

Material	Count [tex]	Nominal strength [cN/tex]
Polyester (PET)	63	20
Aramid	130	219

In the investigation two types of tetraxial technical textile were considered: PET/PET/PET and PET/Aramid/PET hybrid tetraxial textile. Table 1 lists the features of the yarns (PET and Aramid). Additionally, the fabric construction of the tetraxial technical textiles are summarised in Table 2. In the present investigation, yarn material has been varied only in the weft direction.

Table 2. Features of the tetraxial textiles

Yarns [Warp / Weft / Bias]	Areal density [g/m2]	Warp [ends/cm]	Weft [picks/cm]	Bias [threads/cm]
PET / PET / PET	136	6	7	5
PET / Aramid / PET	159	6	7	5

3. Overview of the experimental investigation

3.1. Yarns

Yarn tensile tests (extracted from fabric in warp, weft, and diagonal directions) were performed by INSTRON device with 500 N load cell. The gauge length was 150 mm and testing speed 5 mm/min. Five tests were performed for each yarn direction (warp, weft, diagonal).

The tensile force vs. strain curves of yarns were depicted considering the free length as base length for strain calculation. PET shows a nonlinear behaviour (a), which, since the early loading, is related to rearrangement of fibres and their alignment in the load direction. On the other hand, Aramid has almost linear behaviour until failure point (b).

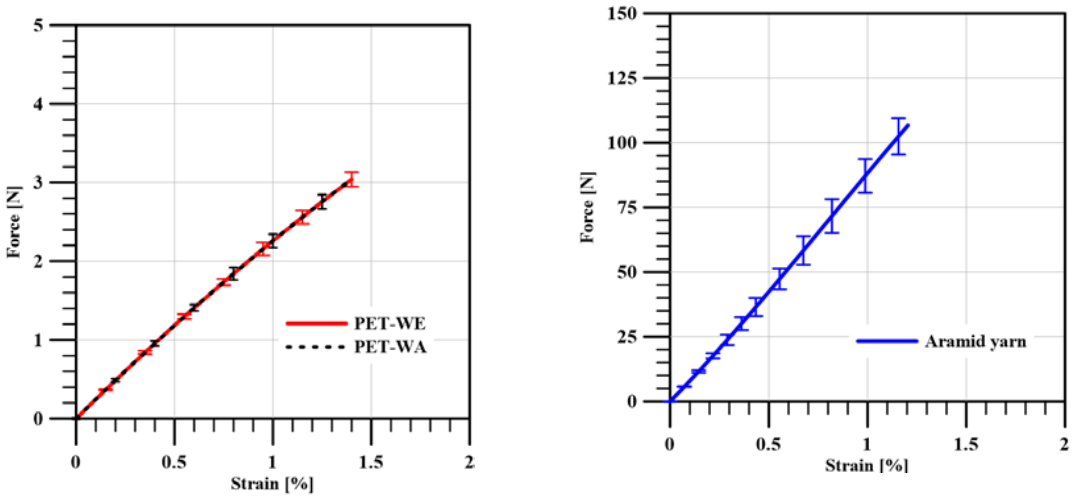

(a) (b)

Figure 3. Force vs. strain curves for yarns extracted from tetraxial fabrics: (a) PET in warp and weft directions, and (b) aramid. Bars indicate standard deviation.

Table 3 collects the average specific strength in warp, weft and diagonal directions for all considered yarns. Special weaving process used to manufacture the tetraxial hybrid fabric has considerable effect on tensile behaviour of some yarns. The comparison of unwoven nominal yarns strength in Table 1and measured in Table 3 of Aramid yarn extracted from weft direction of tetraxial illustrated a significant reduction of strength, while it is slightly changed for weft PET yarn (Figure 3). This is probably due to the intrinsic properties of these materials and the damage induced in the weft path of the weaving loom. Moreover, the weaving loom creates some damage in the warp and diagonal tracks, as well, resulting in

a relative reduction of the PET yarns strength. An in-depth investigation is necessary to better understand the correlation of the yarn material properties and the imparted degradation in the weaving process.

Table 3. Average specific strength of yarns [cN/tex]. (± indicates standard deviation)

	PET	Aramid
Warp yarn	17.56 ± 1.8	-
Weft yarn	20.53 ± 0.82	119.81 ± 0.09
Diagonal yarn	17.61 ± 0.6	-

3.2. Fabrics

Biaxial and uniaxial tensile tests have been considered to investigate the mechanical properties of tetraxial technical textiles. A home design biaxial device was adopted to evaluate the biaxial tensile behaviour. The displacement is generated in each direction of cross-shaped specimen (Figure 4a), which is set in the centre of the machine. Arms of the specimens had width of 100 mm to create a biaxial loaded portion of 100 × 100 mm^2 with an almost uniform distribution of strain on centre part. All tests were performed at room temperature and speed of 1mm/min.

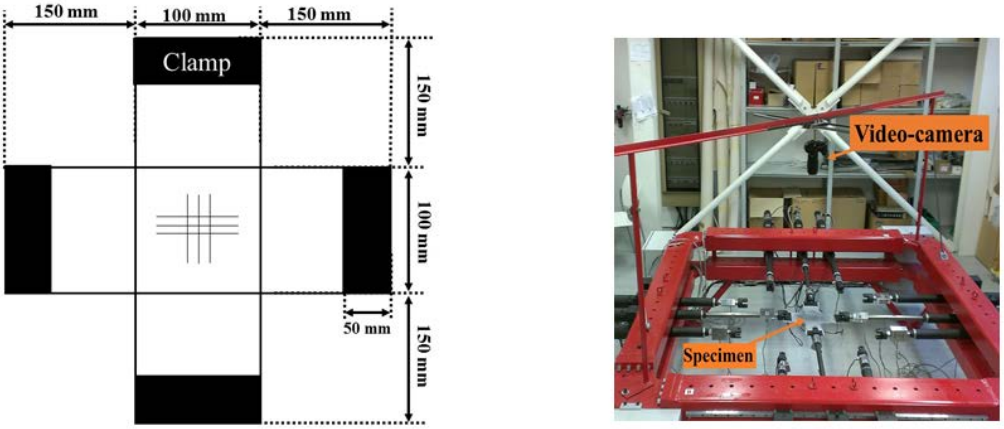

Figure 4. (a) Cross-shaped fabric specimen dimensions, (b) device for biaxial tensile tests.

In order to evaluate the in-plane shear behaviour of tetraxial textiles, bias-extension tests were performed. A tensile test involves rectangular specimen of material such that the warp and weft directions of the yarns are orientated initially at ±45° to the direction of the applied tension load Tabs 3 mm thick, 140 mm wide, and 60 mm long were glued at ends of the specimens, having 280 mm free length between the grips, which give a ratio $\lambda = H_0 / W_0$ of 2. Tests were conducted by an INSTRON device with a speed of 10 mm/min. During test, a digital camera records photograms at a frequency of 1 Hz for image correlation analysis. Post processing by Digital Image Correlation (DIC) [6] allowed estimation of the in-plane shear deformation on the reinforcement surface.

4. Finite element model

To define the constitutive law, it is essential to describe the specific deformation modes of the yarn by a phenomenological approach based on experimental observations. According to [5] four deformation modes, which are related to the behaviour of the yarns and their interaction, are considered: the

elongation in the fibre direction, the compaction of the transverse section of the yarn, the transverse section and the longitudinal shear (Figure 5).

4.1. Hyperelastic constitutive equation

In order to define a hyperelastic material, an elastic strain energy potential per unit volume *w* must exist which depends on the current strain state. To ensure that this constitutive equation fulfils the principle of material frame indifference, a function $\tilde{w}$ of the right Cauchy Green deformation tensor $\underline{\underline{C}}$ must exist.

It has been shown [8] that an isotropic function $\hat{w}$ exists which depends on the right Cauchy-Green strain tensor $\underline{\underline{C}}$ and structural tensors $\underline{\underline{G}}_i$ defining the symmetry group, such as:

$$\tilde{w}\left(\underline{\underline{C}}\right) = \hat{w}\left(\underline{\underline{C}}, \underline{\underline{G}}_i\right) \tag{1}$$

The representation theorems for transversely isotropic functions of scalars, vectors and/or symmetric tensor variables define a finite number of scalar functions ($I_1, ..., I_n$) and a function *w* such as:

$$\hat{w}\left(\underline{\underline{C}}, \underline{\underline{G}}_i\right) = \hat{w}\left(I_1, ..., I_n\right) \tag{2}$$

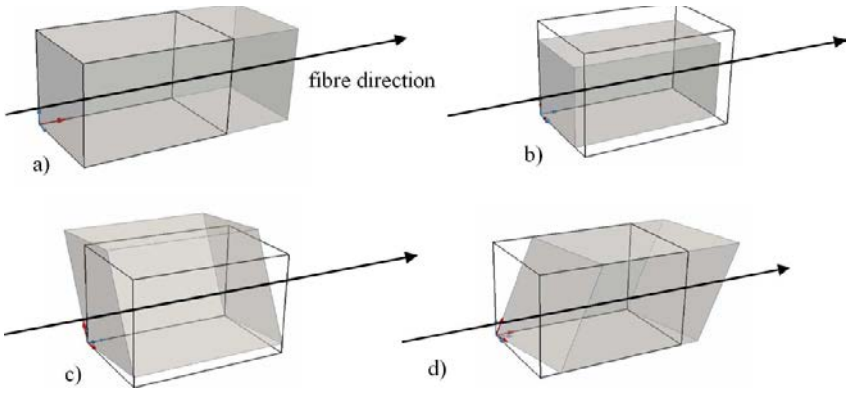

Figure 5. Four different deformation modes of single yarn: (a) elongation, (b) compaction of the cross section, (c) distortion of the cross section and (d) longitudinal shear.

Number *n* depends on the number and type of arguments of the isotropic function under consideration. The symmetry group of a transversely isotropic material is defined, in the initial configuration with a preferred unit direction $\underline{A}$. This allows the definition of a structural tensor $\underline{\underline{A}} = \underline{A} \otimes \underline{A}$. Then, the strain energy potential become:

$$w^{it} = w^{it}\left(I_1, I_2, I_3, II_4, II_5\right) \tag{3}$$

where I_1, I_2, I_3 are the classical invariants of $\underline{\underline{C}}$. II_4 and II_5 are mixed invariants defined from the structural tensor $\underline{\underline{A}}$ by:

$$II_4 = \underline{\underline{C}} : \underline{\underline{A}} = \underline{A} \cdot \underline{\underline{C}} \cdot \underline{A} \quad and \quad II_5 = \underline{\underline{C}}^2 : \underline{\underline{A}} = \underline{A} \cdot \underline{\underline{C}}^2 \cdot \underline{A} \tag{4}$$

4.2. Constitutive equation for a yarn

If $\underline{A}$ is a unit vector, the elongation of the yarn in the direction of the fibres is directly given by invariant II_4 defined in (4). Consequently, this quantity can be chosen as the representative value of the length change of the yarn:

$$I_{elong} = \underline{\underline{C}} : \underline{\underline{A}} \tag{5}$$

Yarn compaction, distortion and longitudinal shear can be characterized using the following expressions [9]:

$$I_{comp} = \sqrt{\frac{I_3}{I_4}} \quad I_{dist} = \sqrt{I_1 - \frac{I_4}{I_5} - 2I_{aire}} \tag{6}$$

The constitutive equation is the summation of all contributions:

$$\underline{\underline{S}} = 2\frac{\partial w}{\partial \underline{\underline{C}}} = 2\left(\frac{\partial w_{elong}}{\partial I_{elong}}\frac{\partial I_{elong}}{\partial \underline{\underline{C}}} + \frac{\partial w_{comp}}{\partial I_{comp}}\frac{\partial I_{comp}}{\partial \underline{\underline{C}}} + \frac{\partial w_{dist}}{\partial I_{dist}}\frac{\partial I_{dist}}{\partial \underline{\underline{C}}}\right) \tag{7}$$

More details can be find in [5]. The constitutive equation has been implemented in a user material subroutine VUMAT for ABAQUS/Explicit finite element code, developed at INSA Lyon [5].

5. Results and comparisons

For each deformation mode (see Figure 5), a strain energy density function based on the experimental behaviour of the technical textile [1], is defined. Afterwards, the strain energy density is used to determine the model parameters by means of a sum of differences squared algorithm, which optimizes the calculated and experimental energies.

5.1. Mesh sensitivity

In Figure 6, two types of mesh are proposed to check the mesh sensitivity. The force vs. logarithmic strain for both meshes is depicted in Figure 7. This comparison shows that improvement of mesh does not have any substantial effect on the numerical prediction.

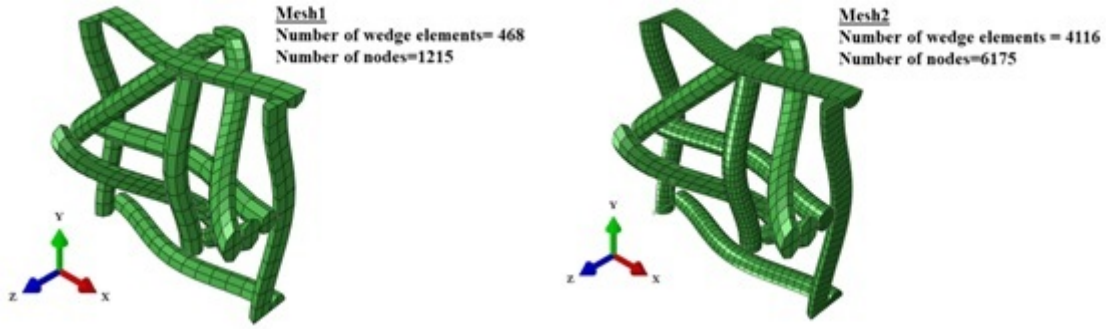

Figure 6. Two different meshes for PET/PET tetraxial unit cell.

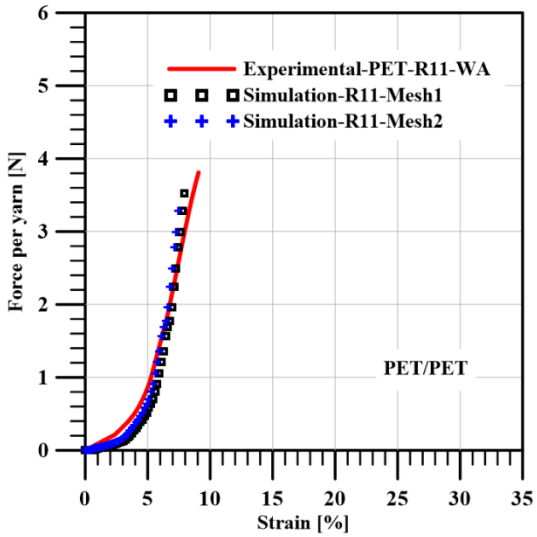

Figure 7. Effect of the refinement of mesh in PET/PET tetraxial hybrid textile.

5.2. Tensile loading

The numerical results were validate by comparison with experimental results of bi-axial tensile loadings. Comparison of bi-axial tensile test for PET/PET and PET/Aramid tetraxial textiles with different warp to weft displacement ratio *R* is depicted in Figure 8. The good agreement between the experimental and numerical curves for "R11", ''R12'' and ''R21'' validated the proposed hyperelastic constitutive law.

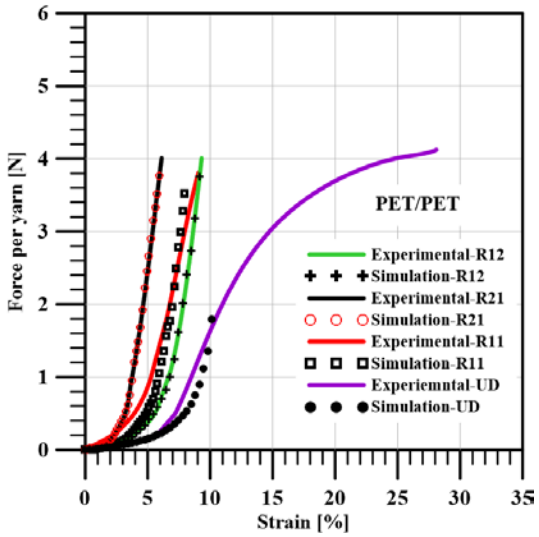

(a)

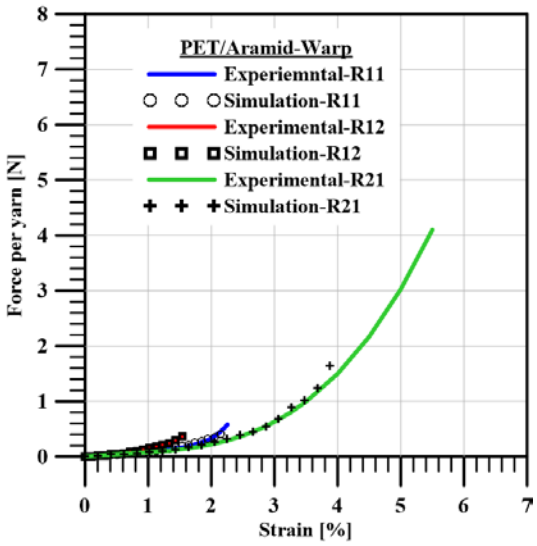

(b)

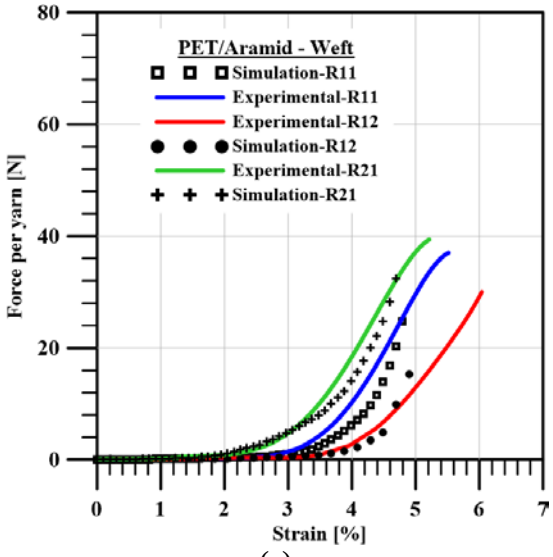

(c)

Figure 8. Comparison of experimental observation and FEA for biaxial loading of hybrid tetraxial technical textile; (a) PET/PET tetraxial textile, (b) PET/Aramid in warp direction, and (b) PET/Aramid in weft direction.

5.3. Shear Loading

Figure 9 presented the comparison of FEA and experimental observation for bias extension test. The force vs. in-plane shear deformation curves show a significant agreement between experimental and numerical results. Comparisons in Figure 9a,b illustrated that changing the yarn material in weft direction has not any significant effect on in-plane deformation of hybrid tetraxial textiles, and this point is evident with the numerical results too.

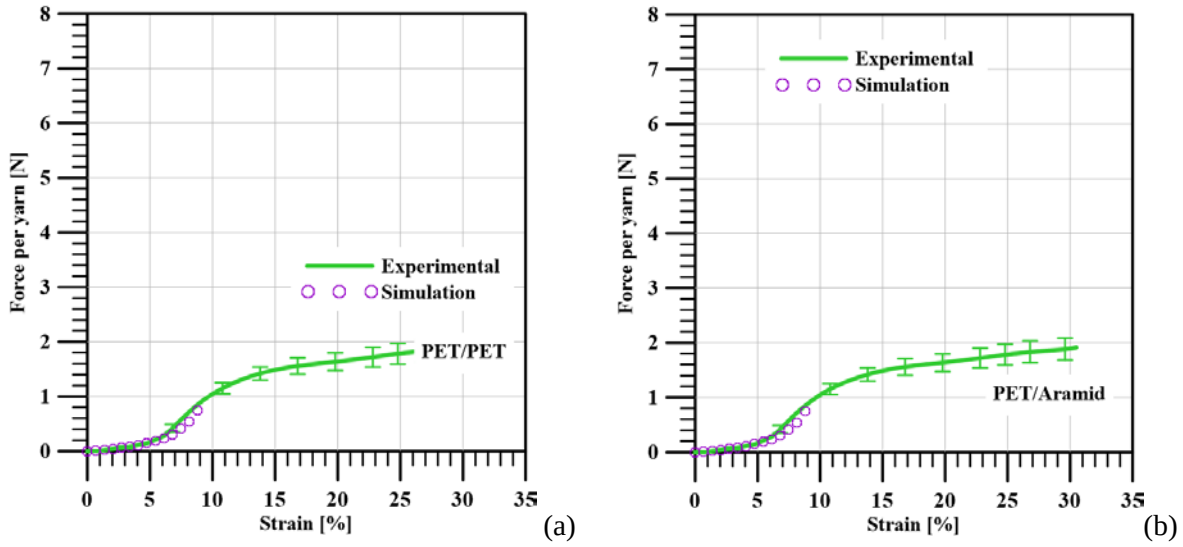

Figure 9. Comparison of experimental observation and FEA results for bias extension loading of tetraxial technical textiles: (a) PET/PET and (b) PET/Aramid.

6. Conclusions

Comparison of meso-scale FE analyses and experimental results of in-plane deformations of tetraxial technical textiles (PET/PET and PET/Aramid) based on a hyperelastic constitutive law has been presented. To validate the meso-scale finite element modelling the simulation of the unequal and equi-biaxial tensile loading of a representative unit cell is performed. The numerical and experimental results have a substantial good agreement. Moreover, numerical results of in-plane shear loading of PET/PET and PET/Aramid tetraxial textiles have also a significant agreement with experimental measurements.

Acknowledgements

The work was supported by the Italian Ministry of Economic Development under the research project 'Tetraxial' (Grant No. MI01_00202).

References

[1] M. Ghazimoradi, V. Carvelli, M. C. Marchesi, and R. Frassine, "Mechanical characterization of tetraxial textiles," *J. Ind. Text.*
[2] J. Pazmino, V. Carvelli, and S. V. Lomov, "Formability of a non-crimp 3D orthogonal weave E-glass composite reinforcement," *Compos. Sci. Technol.*, vol. 61, pp. 76–83, 2014.
[3] S. C. Quek, A. M. Waas, K. W. Shahwan, and V. Agaram, "Analysis of 2D triaxial flat braided textile composites," *Int. J. Mech. Sci.*, vol. 45, no. 6–7, pp. 1077–1096, 2003.
[4] F. Loix, P. Badel, L. Orgéas, C. Geindreau, and P. Boisse, "Woven fabric permeability: From textile deformation to fluid flow mesoscale simulations," *Compos. Sci. Technol.*, vol. 68, no. 7–8, pp. 1624–1630, 2008.
[5] A. Charmetant, E. Vidal-Sallé, and P. Boisse, "Hyperelastic modelling for mesoscopic analyses of composite reinforcements," *Compos. Sci. Technol.*, vol. 71, no. 14, pp. 1623–1631, 2011.
[6] "Correlated Solutions, Inc., VIC-2D, Irmo, SC, USA," 2012. [Online]. Available: http://www.correlatedsolutions.com.
[7] A. Charmetant, J. G. Orliac, E. Vidal-Salle and P. Boisse, "Hyperelastic model for large deformation analyses of 3D interlock composite preforms," *Compos. Sci. Technol.*, vol. 72, no. 12, pp. 1352–1360, 2012.
[8] Q.-S. Zheng, "Theory of Representations for Tensor Functions—A Unified Invariant Approach to Constitutive Equations," *Appl. Mech. Rev.*, 1994.
[9] J. C. Criscione, A. S. Douglas, and W. C. Hunter, "Physically based strain invariant set for materials exhibiting transversely isotropic behavior," *J. Mech. Phys. Solids*, 2001.